



On the asymmetry of Nathair Facula, Mercury

David A. Rothery^{a,*}, Océane Barraud^b, Sebastien Besse^c, Cristian Carli^d, David L. Pegg^a, Jack Wright^a, Francesca Zambon^d

^a School of Physical Sciences, The Open University, Milton Keynes MK7 6AA, UK

^b LESIA, Observatoire de Paris, Université PSL, CNRS, Sorbonne Université, Université de Paris, 5 place Jules Janssen, Meudon 92195, France

^c Aurora Technology B.V. for ESA, European Space Agency, Madrid, Spain

^d INAF, Istituto di Astrofisica e Planetologia Spaziali (IAPS), Via del Fosso del Cavaliere, Rome 00133, ITALY

ARTICLE INFO

Keywords:
Mercury
Eruption
Explosive
Spectral
Vent

ABSTRACT

Nathair Facula is the largest and most spectrally distinct of nearly 200 ‘bright red’ spots (faculae) on Mercury’s surface, most of which are accepted to be deposits from explosive volcanic eruptions. Like most of Mercury’s faculae, it hosts a non-circular central pit (in this case nearly 40 km wide and 3 km deep). However, the center of this facula does not coincide with its central pit’s midpoint. Quantitative analysis of two sets of spectral data shows that the facula’s midpoint is offset by 10–30 km northwards or northeastwards, and probably lies outside the pit. The pit area is almost certainly a ‘compound vent’, within which the locus of eruption has migrated between eruptive episodes. The asymmetry of the facula and the texture of the vent floor are consistent with the most energetic and/or the most recent eruptions having occurred from the northeastern part of the compound vent, but evidence that the center point of the facula lies outside the vent indicates that it may be necessary to invoke an additional factor such as asymmetric eruption fountains.

1. Introduction

Faculae on Mercury are high-albedo, spectrally red, surficial deposits typically tens of km in diameter that have indistinct outer edges. They have been described in several studies (Blewett et al., 2009; Kerber et al., 2009, 2011; Goudge et al., 2014; Thomas et al., 2014) using data from the MErcury Surface, Space ENvironment, GEochemistry, and Ranging (MESSENGER) mission (Solomon et al., 2007), particularly its Mercury Dual Imaging System, MDIS (Hawkins et al., 2007). This had a single channel (700–800 nm) narrow angle camera (NAC) and a wide angle camera (WAC) imaging in up to 11 colors from 430 to 1020 nm.

At first, Mercury’s faculae were usually referred to as a ‘red spots’, until 2018 when the IAU (International Astronomical Union) approved the use of the descriptor term ‘facula’. At the center of most faculae is a non-circular ‘rimless’ pit, lacking a surrounding raised rampart but delimited instead by a ‘brink’ where the ground drops away into the pit. Pits are several km across and typically more than 1 km deep. Faculae surrounding such pits are widely accepted as ejecta deposits of explosive volcanic eruptions from vents now marked by the pit. Faculae lacking an obvious major pit, notably the red pitted ground of Thomas et al. (2014), probably have a different origin such as passage of lava across volatile-

rich substrate.

Nathair Facula (Fig. 1) is the largest facula on Mercury. Before its formal name was allocated it was often referred to as ‘NE Rachmaninoff’ (e.g. Kerber et al., 2011) because it lies about 200 km beyond the northeast rim of the named crater Rachmaninoff, whereas Jozwiak et al. (2018) identify it as ‘Copland-Rachmaninoff’. The radius of this facula was conservatively estimated at 71 km by Kerber et al. (2009) when first seen in MDIS images from MESSENGER’s first flyby. However, subsequent orbital imagery showed it to be larger. Thomas et al. (2014) described it as having a 130 km radius (Fig. 2a), the first quadrangle geological map containing it (Fig. 3; Wright et al., 2019) portrays it with a 120 km radius, and Besse et al. (2020) employed more objective measures using spectral data from a north–south MASCS profile to demonstrate a radius of 140 km. Although the Nathair Facula vent was blasted through relatively old intercrater plains, much younger age constraints can be inferred because in places the facula overlies both smooth plains and ejecta from the class *c*₄ crater Rachmaninoff (Wright et al., 2019; Kinczyk et al., 2020). This makes the facula Mansurian or younger in age, which is almost certainly younger than 1.7 Ga and possibly younger than 0.85 Ga (Banks et al., 2017).

If a facula is the product of explosive volcanism, then the dispersal

* Corresponding author.

E-mail address: d.a.rothery@open.ac.uk (D.A. Rothery).

<https://doi.org/10.1016/j.icarus.2020.114180>

Received 6 August 2020; Received in revised form 16 October 2020; Accepted 21 October 2020

Available online 27 October 2020

0019-1035/© 2020 The Authors.

Published by Elsevier Inc.

This is an open access article under the CC BY-NC-ND license

(<http://creativecommons.org/licenses/by-nc-nd/4.0/>).

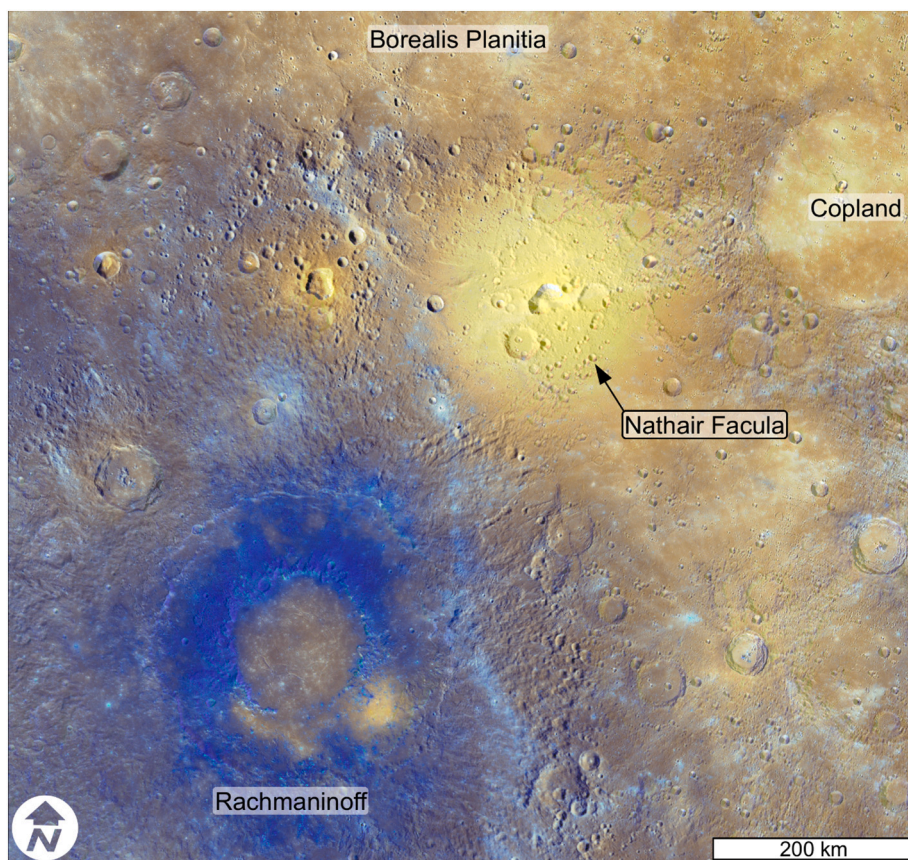


Fig. 1. Nathair Facula in its regional setting, seen in enhanced MESSENGER color. This is a standard 665 m/pixel product, derived by principal component (PC) analysis of MDIS WAC data (red = PC2, green = PC1, blue = 433 nm/996 nm), overlain with 50% transparency over a 166 m/pixel NAC monochrome basemap. Nathair Facula is the yellow spot in excess of 200 km diameter centered near 35° N, 64° E. Rachmaninoff and Copland are two named craters. This is a stereographic projection centred on 63.8°E, 35.8°N, which is the notional center of the facula's compound vent. (For interpretation of the references to color in this figure legend, the reader is referred to the web version of this article.)

range can be used to estimate gas content at the seat of the eruption (Kerber et al., 2009; Thomas et al., 2014; Weider et al., 2016). Having been given their initial velocity during ejection from the vent by gas expansion, the explosive ejecta particles would have travelled on ballistic trajectories in conditions very near to a vacuum (Wilson and Head III, 1981). The large size of Mercury's faculae has been used as evidence to support the consensus that Mercury (or at least its crust, if that is their source) is rich in volatiles (e.g., Kerber et al., 2009). Although the dimensions of a facula are controlled primarily by the explosivity of the eruption, we expect its apparent size to increase slightly (for a fixed explosivity) with the duration of eruption because the facula's spectral contrast with its surroundings, especially in its more transparent outer parts, would intensify as more volcanic ejecta accumulated. These arguments remain broadly valid even for a facula that may be the cumulative product of a series of eruptions, which is particularly likely in the case of any facula whose central pit rather than being simple, is a compound structure comprising multiple overlapping vents.

The first compound vent on Mercury to be described in detail (Rothery et al., 2020) is in the southwest of the Caloris basin, and its surrounding deposit now bears the name Agwo Facula. Pegg et al. (submitted) have shown that about 70% of vent sites on Mercury fall into the 'compound vent' category.

Here we consider the size and shape of Nathair Facula, which also surrounds a compound vent. Being the largest example of its kind on Mercury, it is the one most amenable to study with MESSENGER data, and gives a foretaste of issues that could be probed more widely and deeply by the more diverse and higher resolution instruments carried by BepiColombo, which is now en route to begin orbital science about Mercury in 2026 (Benkhoff et al., 2020; Milillo et al., 2020; Rothery et al., 2020). We present evidence that Nathair Facula's mid-point does not coincide with the middle of its pit structure, and discuss the possible reasons for these observations.

2. The Nathair Facula vent area

Nathair Facula surrounds the largest recognised vent structure on Mercury. This is a pit measuring 39 km on its long axis (oriented east-northeast–west-southwest) and 30 km on its short axis (Fig. 4). Thomas et al. (2014) used a digital elevation model (DEM) to calculate the volume of the pit as 1268 km³. As shown by Thomas et al. (2014), the brink of this pit is raised only subtly above the level of the pre-existing surrounding terrain, by about 200 m, whereas inside it plunges steeply (at about 30°) to an uneven floor more than 2 km below, with a greatest depth of about 3 km (Fig. 2b,c). In plan view the brink is non-elliptical, having some sectors whose curvature is convex inwards that alternate with more strongly curved convex-outward sectors (Fig. 4b). Unlike most compound vents there are no clear septa (narrow internal topographic partitions) between individual vents, but there are three closed depressions on the floor separated by broad rises. The floor has marked changes in texture, corresponding with the more subtle changes in level that define the depressions, which may record migration of the locus of explosive activity over time. These features suggest that the vent is probably compound, although less clearly so than many other compound vents on Mercury (Pegg et al., 2020(submitted)). The general form of the overall pit is more consistent with having been excavated explosively than by piston-like subsidence on caldera-bounding ring faults (as is common on Earth and Mars, e.g. Howard, 2010). It is notable that the roughest area of the entire floor is in the northeast (Fig. 4 c,d). The more muted texture of other parts of the floor can be explained by mantling by proximal deposits except in the rough northeastern area, which was thus probably the seat of the final eruption.

3. The composition of Nathair Facula

Although grain-size could play a role (Braden and Robinson, 2013;

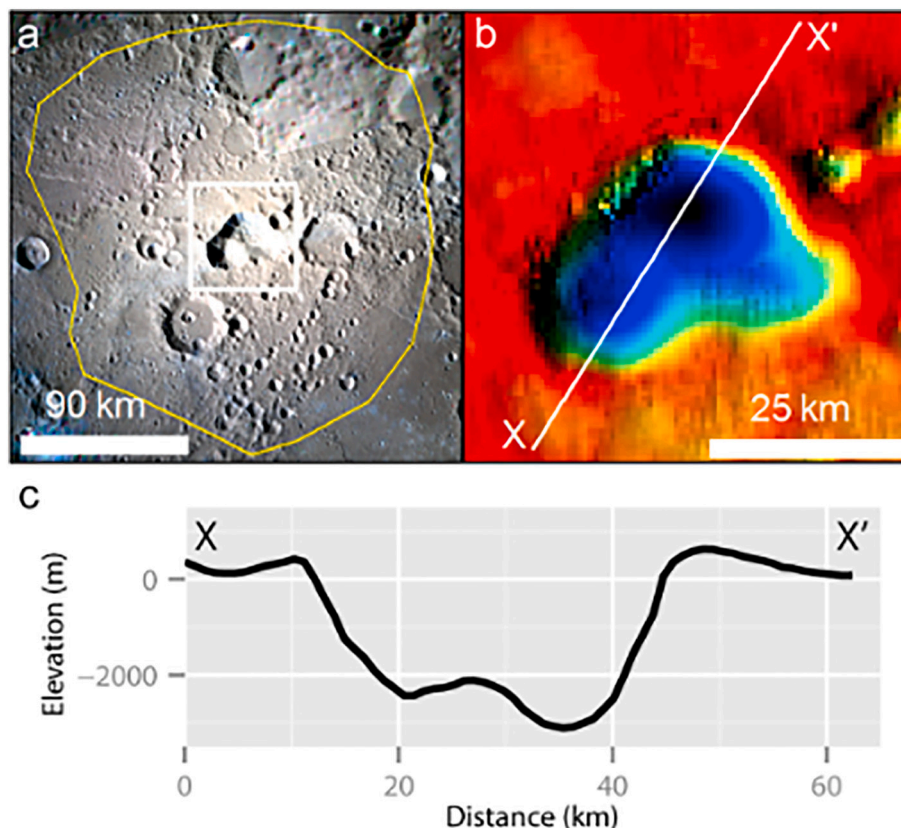


Fig. 2. Nathair Facula and its vent as documented in [Thomas et al. \(2014\)](#). (a) Unenhanced MDIS color composite with the approximate visual extent of the facula outlined. (b) Hill-shaded stereo-derived DEM of the area within the box in (a). (c) Topographic section along the line X–X' in (b). [Thomas et al. \(2014\)](#) attributed the excess height of the rim in the NE to a pre-existing thrust-related ridge.

[Gouge et al., 2014](#)), the spectral distinctiveness of Mercury's faculae is more widely-regarded (e.g., [Zolotov, 2011](#); [Peplowski et al., 2016](#); [Weider et al., 2016](#); [Nittler et al., 2020](#)) as being largely because volatiles (whose presence would increase the explosivity of the magma) have been stripped away from the ejecta during eruption. In the case of Nathair Facula, there is evidence to support this contention, because it is the only facula big enough for MESSENGER to have been able to determine elemental composition. It was overflowed during a targeted 'staring mode' conducted by MESSENGER's X-Ray Spectrometer (XRS; [Schlemm et al., 2007](#)) at a time when X-ray fluorescence was enhanced because of a powerful solar flare. The high flux and 200 s integration time allowed spatially resolved elemental ratio measurements of the facula. These revealed a Ca/S ratio five times higher than the global mean, taken to demonstrate depletion of sulfur in the deposit ([Weider et al., 2016](#); [Nittler et al., 2020](#)). There is also an apparent depletion of carbon, inferred from a decrease in thermal neutron count rates over the facula detected by MESSENGER's Gamma-Ray and Neutron Spectrometer (GRNS; [Goldsten et al., 2007](#)), which is indicative of carbon also having been lost ([Peplowski et al., 2016](#)). This is consistent with [McCubbin et al. \(2017\)](#) who argue that a smelting reaction between silicates and graphite could potentially make CO the dominant volcanic gas. [Weider et al. \(2016\)](#) reasonably interpret these results as indicating that both S and C were lost during eruption, most likely by oxidation reactions liberating sulfur and carbon oxides as the expanding gases that drove the explosive eruption, although [Li et al. \(2017\)](#) argue that that under reducing conditions the main volcanic gas is most likely to have been CH₄.

4. The thickness and extent of Nathair Facula

A facula is a surficial deposit, mostly too thin to obscure pre-existing

small impact craters but visible because its spectral properties contrast with the underlying unit. [Thomas et al. \(2014\)](#) measured slopes outside the perimeter of the Nathair Facula pit. They suggested a proximal deposit thickness of 100–200 m with an initial outward slope of about 2°, which becomes imperceptibly thin at a range greater than about 10 km. [Brož et al. \(2018\)](#) showed that wide dispersal of ejecta and consequent lack of a major edifice around the vent is to be expected under Mercury's airless and low-gravity conditions.

We note here that a 100 m thick deposit surrounding the pit to a distance of 10 km from its brink would have a volume of about 150 km³. If the total volume in the facula is approximately equal to the empty volume of the pit (1268 km³ as reported by [Thomas et al., 2014](#)), this proximal part of the total deposit could account for only about 12% of the total. However, an average thickness of less than 20 m is all that is necessary to account for the remaining 88% in a distal deposit surrounding the proximal part of the deposit out to a radius of 140 km.

Whether a facula's spectral distinctiveness is because of loss of carbon and/or sulfur from the ejected material into the gas phase or because of some other factor is not important in this discussion. Irrespective of its cause, the original visible outer edge of a facula would have been gradational across the radial zone where the cover by volcanic ejecta particles fell from 100% to zero with increasing range. Another factor making the edge of a facula diffuse today is that the spectral distinctiveness of a facula, particularly its thinner distal region, can be expected to decrease over time because of the action of impact gardening in mixing underlying material upwards into the volcanic ejecta deposit (e.g., [Costello et al., 2020](#)). All parts of the facula might also fade over time because of general space weathering processes ([Besse et al., 2020](#)).

Being gradational, the outer edge of a facula is challenging to define in an objective way. [Thomas et al. \(2014\)](#) who outlined the edge of

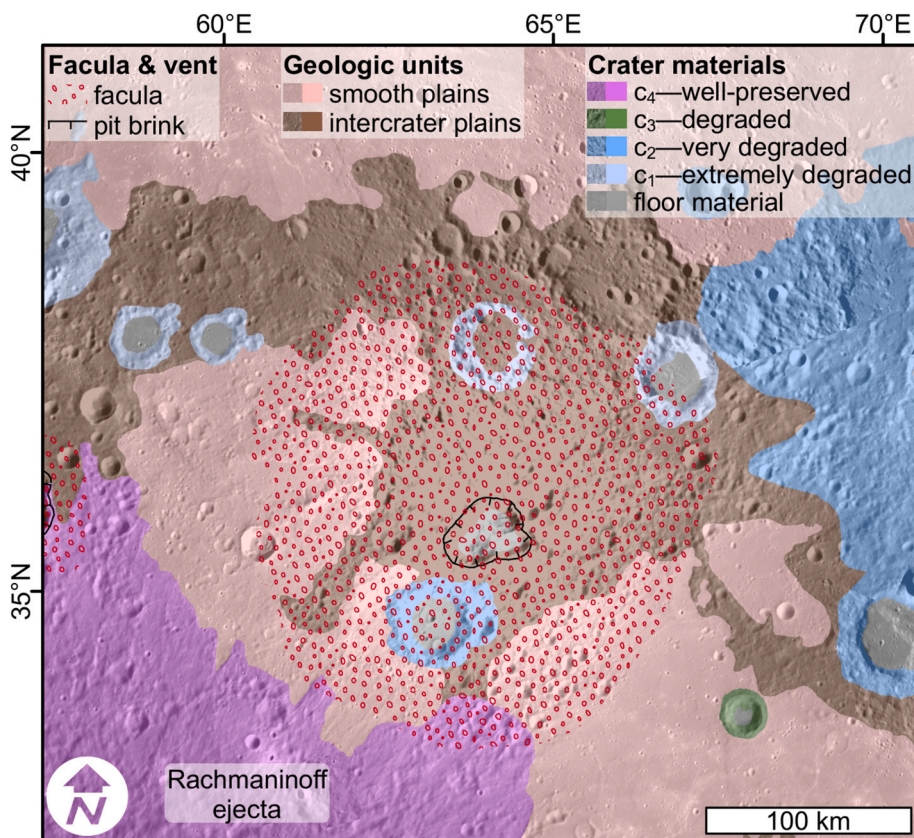


Fig. 3. The extent of Nathair Facula as portrayed on the 1:3 M scale morphostratigraphic map of Wright et al. (2019), which was based on interpretation of MDIS NAC and WAC images. This version is shown with 50% transparency over a 166 m/pixel monochrome basemap. Stereographic projection centred on 63.8°E, 35.8°N.

Nathair Facula (Fig. 2a) and Wright et al. (2019) who showed it slightly smaller in their 1:3 M map of the Hokusai quadrangle (Fig. 3) both identified its limits visually, on the basis of enhanced MESSENGER MDIS images. Rather than fitting a notional circle to it, both attempted to show its true shape by tracing a slightly irregular boundary that defined a roughly equidimensional deposit. The exact position of such a boundary is subjective and is affected by factors such as whether it is drawn on the basis of a monochrome or color image, and on the contrast stretch used for display.

Besse et al. (2020) took a more numerical and repeatable approach to defining the edge of Nathair Facula and several others, using spectroscopic data from the Mercury Atmospheric and Surface Composition Spectrometer (MASCS; McClintock and Lankton, 2007). This was a non-imaging instrument that recorded ultraviolet–visible–near-infrared spectra along the spacecraft ground-tracks. Besse et al. (2020) defined three spectral parameters that are extreme in the inner part of faculae but whose values decrease linearly to the planetary background value at a distance that they interpreted as the edge of the facula: the ultraviolet (UV) downturn, the visible (VIS) slope and the near-infrared (NIR) slope. Along a nearly north–south track across Nathair Facula they used these data to determine a radius of about 140 km, slightly larger than previously published values, beyond which all three spectral parameters tend to stabilise around Mercury’s background values as defined by Izenberg et al. (2014). Unfortunately, MASCS tracks were too widely-spaced to allow the facula’s east-west extent to be constrained in the same manner.

5. The asymmetry of Nathair Facula

Careful inspection of enhanced MESSENGER color images, such as Fig. 1, and the map of Wright et al. (2019, Fig. 3) suggests that the facula is not actually centered on the vent, but is offset northwards by about 20 km. To test this, we interrogated MASCS and MDIS data more

thoroughly.

5.1. MASCS analysis

When Besse et al. (2020) analyzed their north–south MASCS profile across Nathair Facula they focussed on distance from the notional centre of the vent (which they took to be 63.8° W, 35.8° N), irrespective of direction north or south along the track. Here we use the same data but distinguish between data points north and south of the vent, and similarly interrogate MASCS data from four additional north–south crossings of this facula. Two of these are illustrated in Figs. 5 and 6, showing that each spectral parameter falls to the background level at a greater distance to the north than to the south of the notional vent centre.

Table 1 summarizes data from all five tracks. The median radius from these tracks based on UV downturn shows the radius of Nathair Facula (expressed as half the sum of the north+south radii) to be 140.5 km. This agrees with Besse et al.’s (2020) estimate of “about 140 km”. The VIS and NIR slopes show indications of the facula extending even further (radii of about 155 km and 182 km respectively). This is an additional indication of the great extent of this facula and of the difficulties inherent in defining the edge of such a diffuse feature, which blends gradually into the background with increasing range. However, although each spectral parameter records a slightly different radius (usually least for UV-downturn and, where determined, greatest for NIR slope), in all cases where a radius can be determined it is greater to the north than to the south. In the case of the UV downturn (arguably the most robust single measure), the mean and median agree on an approximately 21 km discrepancy between the north and south radii. This would be eliminated if the true center were shifted north of the notional center by about 10 km. This could be within the perimeter of the vent only if situated in the rougher (and therefore probably younger) northeastern part of the vent floor indicated in Fig. 4.

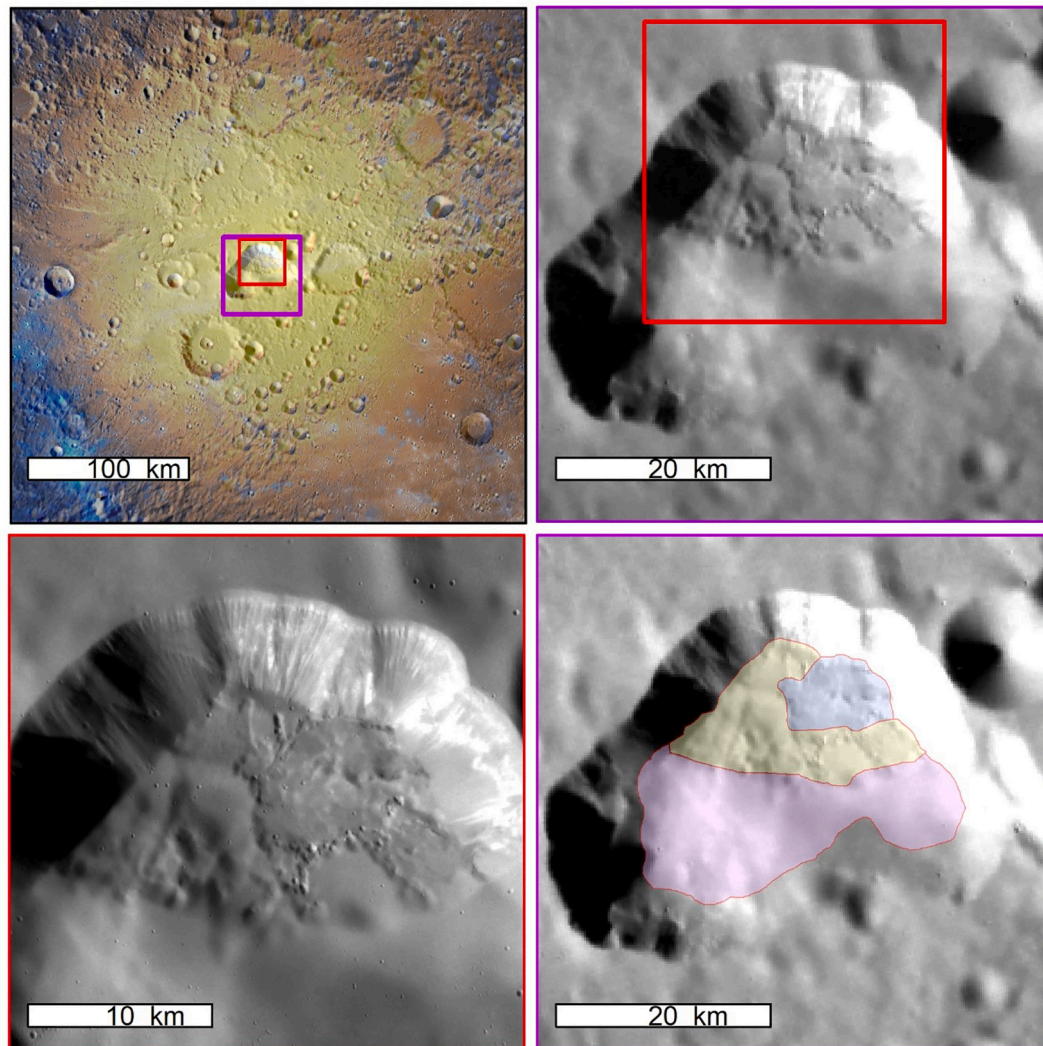


Fig. 4. (a) Enhanced color basemap image of Nathair Facula, similar to Fig. 1. Although there are some issues with shadow on the walls, the floor of the vent complex has distinct spectral properties in common with the facula outside the vent (see section 5.2). The larger, purple box shows the extent of (b) and (d), and the smaller, red box the extent of (c). (b) Overview of the morphology inside the vent complex. The roughest texture is visible in the northeast of the floor, suggesting that this was the most recently active area. Image: EW0254884916G (200 m/pixel). (c) Detail of the northeast part of the vent complex. Image EN0224508427 (37.6 m/pixel). Both images are illuminated from the west. (d) The floor of the entire vent divided into areas based on texture, smoother in the south and rougher in the northeast. Image EW0254884916G. (For interpretation of the references to color in this figure legend, the reader is referred to the web version of this article.)

5.2. MDIS analysis

MASCS analysis confirms and quantifies the north–south asymmetry of the facula, but offers no east–west constraint. We turn now to quantitative analysis of MDIS data to test in two-dimensions both this asymmetry and the earlier visual interpretations of MDIS data. We used multispectral images from the MDIS wide-angle camera (WAC). We processed WAC data of the Nathair Facula region following the methodology of Zambon et al., 2020 (in preparation), with a spatial resolution of 450 m/pixel. We applied the Kaasalainen-Shkuratov photometric correction model with the parameters derived by Domingue et al. (2016), and we normalized images to a standard photometric geometry of 30° incidence angle, 0° emission angle and 30° phase angle with the aid of a 222 m/pixel Digital Elevation Model (DEM) released by DLR (Stark et al., 2017). Any residual latitudinal or longitudinal effects on the visibility of the facula are small enough to be negligible in the analysis that follows.

The spectral shape (normalized to 550 nm) is very similar for all regions, including the vent floor, apart from the vent walls (which may be a residual geometric effect). We found that reflectance in all 8 WAC

channels decreases from the centre of the facula outwards in an approximately circular concentric pattern. A similar pattern is apparent in spectral slopes (whether across the full range 430 to 1000 nm, or subdivided 430 to 560 nm and 750 to 1000 nm), all of which decrease radially outwards. For simplicity here we use just the normalized reflectance in the 750 nm channel (R750) as a tool to investigate the asymmetry of the facula (Fig. 7). Figs. 7b and c show that the facula is quite well defined using a R750 threshold as low as 0.089, which defines a region about 130 km in radius, consistent with size estimates reported in previous sections. This threshold excludes only those pixels whose R750 is more than 10% above the planetary median of 0.072. If the threshold is set incrementally lower than 0.089, the facula can still be identified with a progressively larger radius, but its edges become more ill-defined, until by 0.079 probably as many false positives are being added outside the facula as are being added within the facula.

We show in Table 2 the cumulative area within the facula as defined by each of the R750 thresholds in Fig. 7c, and the calculated position of the centroid for each cumulative area and the parameters of the best-fit ellipse. The positions of these locations are illustrated in Fig. 8. Note that they all plot outside the compound vent. Errors are hard to quantify, but

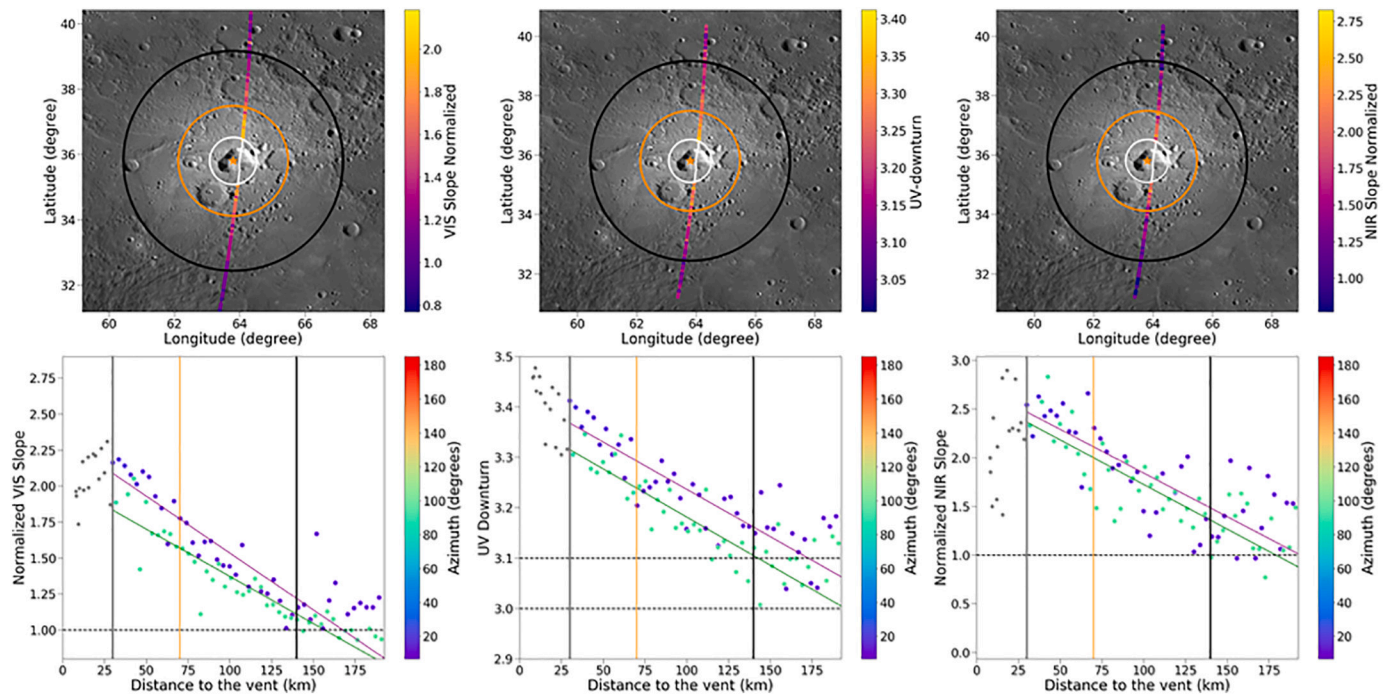


Fig. 5. Variability of the spectral parameters along the orbit ob2_12212_072558. The top three panels represent plan views of the same orbit, with footprints color-coded based on the strength of spectral parameters North is up, corresponding to azimuth 0 or 360. The size of each MASCs footprint is about 500 m across, and the along-track spacing of each measurement is about 3.4 km. The lower three panels display the evolution of each spectral criterion with respect to distance from the notional vent centre, color-coded based on the geographical azimuth from the notional vent centre. These are the data presented in Besse et al. (2020) except that we have fitted separate regression lines to the points north and points south of the vent. The orange and black circles in the top panels, and the corresponding vertical lines in the lower panels, indicate the originally underestimated 70 km radius of the facula (Kerber et al., 2009) and the 140 km radius determined by Besse et al. (2020) assuming a symmetrical facula. Points within the small, innermost, circle encompassing the vent were excluded from the regression analysis.

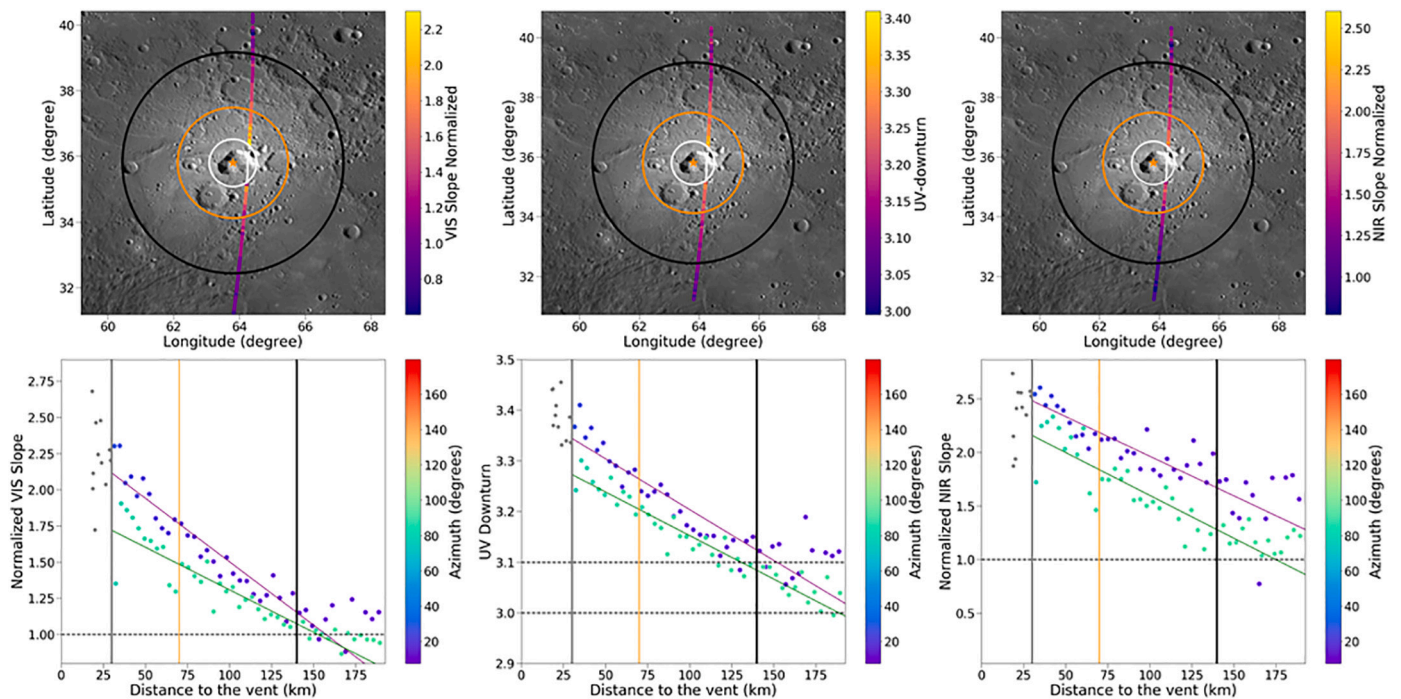


Fig. 6. Variability of the spectral parameters along the orbit orb_12036_191344, presented in the same way as Fig. 5.

are probably about ± 10 km (0.25° in latitude). However, whatever threshold is used, the centroid is consistently always north of the vent's mid-point of 63.8 N, 35.8 E, and for the lower R750 thresholds (which encompass the more distal parts of the facula) the centroid is also further

east and thus close to the youngest part of the vent floor.

Thus, quantitative analysis of MDIS data provides a further clear demonstration that Nathair Facula is not symmetrically disposed relative the compound vent that is its source, and in fact suggests greater

Table 1

North and south radius of Nathair Facula from a notional vent mid-point at 63.8° W, 35.8° N as determined on five MASCS orbital tracks using three spectral parameters: normalized VIS slope, UV-downturn, and normalized NIR slope. The first and second rows of data correspond to Figs. 5 and 6 respectively. Δradius shows the difference between north and south radii, as determined by each spectral parameter. Average radius is half the north-south diameter.

Orbit	Radius North / km			Radius South / km			Δradius / km			Average Radius / km		
	VIS-slope	UV-downturn	NIR-slope	VIS-slope	UV-downturn	NIR-slope	VIS	UV	NIR	VIS	UV	NIR
ob2_12212_072558	168	173	194	157	142	179	11	31	15	162.5	157.5	186.5
orb_12036_191344	157	151	Inconclusive	152	130	Inconclusive	5	21	–	154.5	151.5	–
ob2_12186_223125	159	136	181	140	120	176	19	16	5	149.5	128	178.5
ob2_13021_160023	158	170	Inconclusive	148	164	Inconclusive	10	6	–	153	159	–
orb_12011_053029	198	143	Inconclusive	158	114	Inconclusive	40	29	–	178	150.5	–
Median value / km	159	151	187.5	152	130	177.5	11	21	10	140.5	155.5	182.5
Average value / km	168	154.6	187.5	151	134	177.5	17	20.6	10	159.5	144.3	182.5

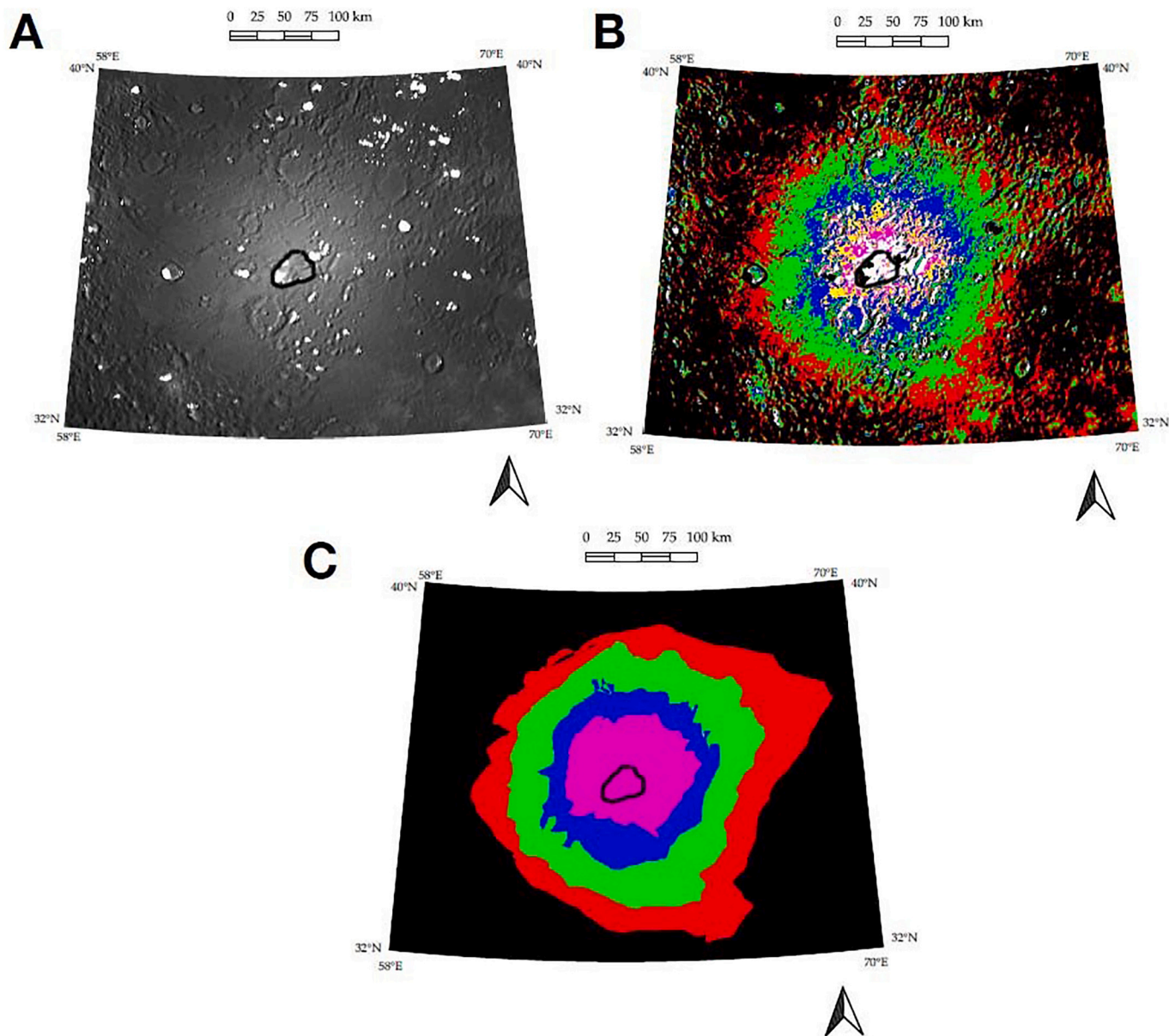


Fig. 7. A reflectance map (R750) of the Nathair Facula region (shadows, where R750 could not be measured, are set to white). B The same area with R750 color-coded in intervals of 10%, 30%, 40%, 50%, 60% and 70% above the planetary median. C The data in B smoothed and with the three innermost (50%, 60% and 70%) classes merged. Colors represent, from the center outwards: magenta R750 > 0.125 (>50% above median), blue R750 0.115–0.125 (40–50% above median), green R750 0.098–0.115 (30–40% above median), red R750 0.089–0.098 (10–30% above median), black R750 < 0.089 (<10% above median). The approximate brink of the pit is shown by the closed black outline near the center of each image. Stereographic projection centred on 63.8°E, 35.8°N. (For interpretation of the references to color in this figure legend, the reader is referred to the web version of this article.)

Table 2

Size and centroid coordinates of Nathair Facula, as defined by various R750 thresholds (see Fig. 7).

R750	% over median value	semimajor axis / km	semiminor axis / km	Centroid Long.	Centroid Lat.	Area /km ²
≥0.089	10	139.5	122.9	64.3° E	36.5° N	55,200
≥0.098	30	114.1	94.5	64.4° E	36.3° N	35,190
≥0.115	40	78.1	71.3	63.6° E	36.3° N	17,272
≥0.125	50	52.4	48.6	63.6° E	36.7° N	8507

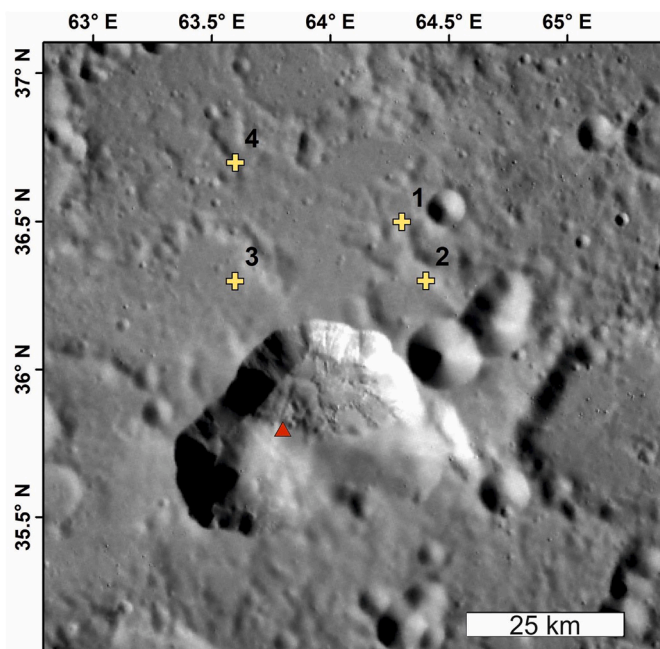


Fig. 8. The locations of the Nathair Facula centroids in Table 2, which all lie beyond the vent. The triangle symbol indicates the notional vent center used by Besse et al. (2020). The MASCS analysis in Table 1 implies that the latitude of the facula mid-point is about 36.03° N.

offset to the north even than the approximately 10 km offset indicated by MASCS analysis. The facula centroids plotted in Fig. 8 do not indicate candidate eruptive sites. All eruptions are highly likely to have been from sites on the floor of the clearly visible compound vent. We discuss below some possible reasons why Nathair Facula is asymmetric.

6. Discussion and conclusions

Nathair Facula is detectable well beyond 100 km from the edge of the pit from which its spectrally-distinct material was erupted. It is close to circular in form, with a slight tendency towards east-west elongation in shape (echoing the elongation of the pit itself). Various methods for defining its outer edge give differing results, but they are all consistent with the center point of the facula lying north or northeast of the middle of the vent area represented by the pit. Quantitative analysis of MDIS data shows that the center point of the facula is actually beyond the brink of the pit. Possible explanations for the asymmetric distribution of this facula are:

1. The facula is a cumulative deposit from multiple sources within the compound vent, and the northeastern eruptions were stronger or more recent. This is consistent with inferences that can be drawn from the spatially-variable roughness of the floor of the compound vent and the plausible notion that a facula can be expected to fade, and hence get smaller, with age.
2. At least some of the eruptions that contributed to the facula were from conduits inclined slightly towards the northeast, so that the

eruptive fountain was asymmetric and sent more ejecta towards the northeast.

3. The facula was originally symmetric, but has been differentially affected by space weathering or partial burial by later impact ejecta.

The third explanation is unlikely, because there is no sign of obscuration by impact ejecta, and studies of other faculae show no weathering dependence on latitude (Besse et al., 2020). We therefore suggest that the asymmetric distribution of Nathair Facula is most likely because of multiple eruptions, but we cannot discount the asymmetric eruption fountain explanation as an additional contributing factor even if this is not the main reason for the facula's asymmetry.

Future studies of the distribution of other faculae with respect to their source vents are likely to prove instructive.

Declaration of Competing Interest

None.

Acknowledgements

Carli, Rothery, Wright and Zambon have received support for this work from the EU Horizon 2020 research and innovation programme under grant agreement No. 776276 (Planmap). Barraud acknowledges the support of Centre national d'études spatiales (CNES). Pegg was funded by the UK Science and Technology Facilities Council (STFC) under grant ST/R504993/1. MESSENGER data are courtesy of NASA/Johns Hopkins University Applied Physics Laboratory/Carnegie Institution of Washington. We thank David Trang for helpful comments at the review stage.

Appendix A. Supplementary data

Supplementary data to this article can be found online at <https://doi.org/10.1016/j.icarus.2020.114180>.

References

- Banks, M.E., Xiao, Z., Braden, S.E., Barlow, N.G., Chapman, C.R., Fassett, C.I., Marchi, S., 2017. Revised constraints on absolute age limits for Mercury's Kuiperian and Mansurian stratigraphic systems. *J. Geophys. Res.* 122 (5), 1010–1020.
- Benkhoff, J., Murakami, G., Baumjohann, W., Besse, S., Bunce, E., Casal, E.M., Cremosese, G., Glassmeier, K.-H., Hayakawa, H., Heyner, D., Hiesinger, H. and 20 others, 2020. BepiColombo – Mission overview and science goals. *Space Sci. Rev.* 216 (in press).
- Besse, S., Doressoundiram, A., Barraud, O., Griton, L., Cornet, T., Muñoz, C., Varatharajan, I., Helbert, J., 2020. Spectral Properties and Physical Extent of Pyroclastic Deposits on Mercury: Variability Within Selected Deposits and Implications for Explosive Volcanism. *J. Geophys. Res.* 125 (5) p.e2018JE005879.
- Blewett, D.T., Robinson, M.S., Denevi, B.W., Gillis-Davis, J.J., Head, J.W., Solomon, S.C., Holsclaw, G.M., McClintock, W.E., 2009. Multispectral images of Mercury from the first MESSENGER flyby: analysis of global and regional color trends. *Earth Planet. Sci. Lett.* 285 (3–4), 272–282.
- Braden, S.E., Robinson, M.S., 2013. Relative rates of optical maturation of regolith on Mercury and the Moon. *J. Geophys. Res.* 118 (9), 1903–1914.
- Brož, P., Cadek, O., Wright, J., Rothery, D.A., 2018. The apparent absence of kilometer-sized pyroclastic volcanoes on Mercury: are we looking right? *Geophys. Res. Lett.* 45 (22), 12–17.
- Costello, E.S., Ghent, R.R., Hirabayashi, M., Lucey, P.G., 2020. Impact Gardening as a Constraint on the Age, Source, and Evolution of Ice on Mercury and the Moon. *J. Geophys. Res.* 125 (3) e2019JE006172.

- Domingue, D.L., Denevi, B.W., Murchie, S.L., Hash, C.D., 2016. Application of multiple photometric models to disk-resolved measurements of Mercury's surface: insights into Mercury's regolith characteristics. *Icarus* 268, 172–203.
- Goldsten, J.O., Rhodes, E.A., Boynton, W.V., Feldman, W.C., Lawrence, D.J., Trombka, J. I., Smith, D.M., Evans, L.G., White, J., Madden, N.W., Berg, P.C., 2007. The MESSENGER gamma-ray and neutron spectrometer. In: *The Messenger Mission to Mercury*. Springer, New York, NY, pp. 339–391.
- Goudge, T.A., Head, J.W., Kerber, L., Blewett, D.T., Denevi, B.W., Domingue, D.L., Gillis-Davis, J.J., Gwinner, K., Helbert, J., Holsclaw, G.M., Izenberg, N.R., 2014. Global inventory and characterization of pyroclastic deposits on Mercury: new insights into pyroclastic activity from MESSENGER orbital data. *J. Geophys. Res.* 119 (3), 635–658.
- Hawkins, S.E., Boldt, J.D., Darlington, E.H., Espiritu, R., Gold, R.E., Gotwols, B., Kardian, C.J., 2007. The Mercury dual imaging system on the MESSENGER spacecraft. *Space Science Reviews* 131 (1), 247–338.
- Howard, K.A., 2010. Caldera collapse: perspectives from comparing Galápagos volcanoes, nuclear-test sinks, sandbox models, and volcanoes on Mars. *GSA Today* 20 (10), 4–10.
- Izenberg, N.R., Klima, R.L., Murchie, S.L., Blewett, D.T., Holsclaw, G.M., McClintock, W. E., Malaret, E., Mauzeri, C., Vilas, F., Sprague, A.L., Helbert, J., 2014. The low-iron, reduced surface of Mercury as seen in spectral reflectance by MESSENGER. *Icarus* 228, 364–374.
- Jozwiak, L.M., Head, J.W., Wilson, L., 2018. Explosive volcanism on Mercury: analysis of vent and deposit morphology and modes of eruption. *Icarus* 302, 191–212.
- Kerber, L., Head, J.W., Solomon, S.C., Murchie, S.L., Blewett, D.T., Wilson, L., 2009. Explosive volcanic eruptions on Mercury: eruption conditions, magma volatile content, and implications for interior volatile abundances. *Earth Planet. Sci. Lett.* 285 (3–4), 263–271.
- Kerber, L., Head, J.W., Blewett, D.T., Solomon, S.C., Wilson, L., Murchie, S.L., Domingue, D.L., 2011. The global distribution of pyroclastic deposits on Mercury: The view from MESSENGER flybys 1–3. *Planet. Space Sci.* 59 (15), 1895–1909.
- Kinczyk, M.J., Prockter, L.M., Byrne, P.K., Susorney, H.C., Chapman, C.R., 2020. A morphological evaluation of crater degradation on Mercury: revisiting crater classification with MESSENGER data. *Icarus* 113637.
- Li, Y., Dasgupta, R., Tsuno, K., 2017. Carbon contents in reduced basalts at graphite saturation: implications for the degassing of Mars, Mercury, and the Moon. *J. Geophys. Res.* 122 (6), 1300–1320.
- McClintock, W.E., Lankton, M.R., 2007. The Mercury atmospheric and surface composition spectrometer for the MESSENGER mission. *Space Sci. Rev.* 131 (1–4), 481–521.
- McCubbin, F.M., Vander Kaaden, K.E., Peplowski, P.N., Bell, A.S., Nittler, L.R., Boyce, J. W., Evans, L.G., Keller, L.P., Elardo, S.M., McCoy, T.J., 2017. A low O/Si ratio on the surface of Mercury: evidence for silicon smelting? *J. Geophys. Res.* 122 (10), 2053–2076.
- Milillo, A., Fujimoto, M., Murakami, G., Benkhoff, J., Zender, J., Aizawa, S., Dósa, M., Griton, L., Heyner, D., Ho, G., Imber, S.M., 68 others, 2020. Investigating Mercury's environment with the two-spacecraft BepiColombo mission. *Space Sci. Rev.* 216 (5), 93. <https://doi.org/10.1007/s11214-020-00712-8>.
- Nittler, L.R., Frank, E.A., Weider, S.Z., Crapster-Pregont, E., Vorbürger, A., Starr, R.D., Solomon, S.C., 2020. Global Major-Element Maps of Mercury from Four Years of MESSENGER X-Ray Spectrometer Observations. *Icarus*, p. 113716.
- Pegg, D., Rothery, L., Balme, M.R., Conway, S.J., 2020. Explosive vent sites on Mercury: commonplace multiple eruptions and their implications. *Icarus* under review ICARUS-D-20-00289.
- Peplowski, P.N., Klima, R.L., Lawrence, D.J., Ernst, C.M., Denevi, B.W., Frank, E.A., Goldsten, J.O., Murchie, S.L., Nittler, L.R., Solomon, S.C., 2016. Remote sensing evidence for an ancient carbon-bearing crust on Mercury. *Nat. Geosci.* 9 (4), 273–276.
- Rothery, D.A., Massironi, M., Alemanno, G., Barraud, O., Besse, S., Bott, N., Brunetto, R., Bunce, E., Byrne, P., Capaccioni, F., Capria, M.T., 55 others, 2020. Rationale for BepiColombo studies of Mercury's surface and composition. *Space Sci. Rev.* 216 (4), 66. <https://doi.org/10.1007/s11214-020-00694-7>.
- Schlemm, C.E., Starr, R.D., Ho, G.C., Bechtold, K.E., Hamilton, S.A., Boldt, J.D., Boynton, W.V., Bradley, W., Fraeman, M.E., Gold, R.E., Goldsten, J.O., 2007. The X-ray spectrometer on the MESSENGER spacecraft. In: *The Messenger Mission to Mercury*. Springer, New York, NY, pp. 393–415.
- Solomon, S.C., McNutt, R.L., Gold, R.E., Domingue, D.L., 2007. MESSENGER mission overview. *Space Sci. Rev.* 131 (1–4), 3–39.
- Stark, A., Preusker, F., Oberst, J., Matz, K.-D., Gwinner, K., Roatsch, T., 2017. High-resolution topography from MESSENGER orbital stereo imaging - the H5 quadrangle "Hokusai". In: *48th Lunar and Planetary Science Conference, The Woodlands, Houston, Abstract #2287*. https://pds-imaging.jpl.nasa.gov/data/messenger/MDIS/MDIS/MESSDEM_1001/DEM/QUAD/IMG.
- Thomas, R.J., Rothery, D.A., Conway, S.J., Anand, M., 2014. Mechanisms of explosive volcanism on Mercury: implications from its global distribution and morphology. *J. Geophys. Res.* 119 (10), 2239–2254.
- Weider, S.Z., Nittler, L.R., Murchie, S.L., Peplowski, P.N., McCoy, T.J., Kerber, L., Klimczak, C., Ernst, C.M., Goudge, T.A., Starr, R.D., Izenberg, N.R., 2016. Evidence from MESSENGER for sulfur- and carbon-driven explosive volcanism on Mercury. *Geophys. Res. Lett.* 43 (8), 3653–3661.
- Wilson, L., Head III, J.W., 1981. Ascent and eruption of basaltic magma on the Earth and Moon. *J. Geophys. Res.* 86 (B4), 2971–3001.
- Wright, J., Rothery, D.A., Balme, M.R., Conway, S.J., 2019. Geology of the Hokusai quadrangle (H05), Mercury. *J. Maps* 15 (2), 509–520.
- Zambon, F. et al. 2020 in prep.
- Zolotov, M.Y., 2011. On the chemistry of mantle and magmatic volatiles on Mercury. *Icarus* 212 (1), 24–41.